Article

Influence of Impregnation Medium on the Adsorptive Performance of Silica Sulfuric Acid for the Removal of Gaseous *o*-Xylene: Comparison on Ethyl Acetate and Water

Dandan Zhao [1,†], Mengze Ma [1,†], Jinjin Qian [1], Yaxu Wang [1], Zichuan Ma [1,*] and Xiaolong Ma [2,*]

1 Hebei Key Laboratory of Inorganic Nano-Materials, College of Chemistry and Material Sciences, Hebei Normal University, Shijiazhuang 050024, China; zhaoddv@163.com (D.Z.); mamengze03@163.com (M.M.); qianjinjin0209@163.com (J.Q.); 18832050289@163.com (Y.W.)
2 School of Environmental Science and Engineering, Hebei University of Science and Technology, Shijiazhuang 050018, China
* Correspondence: mazc@hebtu.edu.cn (Z.M.); maxiaolong2410@hebust.edu.cn (X.M.); Tel.: +86-0311-80787400 (Z.M.)
† These authors contributed equally to this work.

Abstract: Silica supported sulfuric acid (SSA) has been demonstrated to be capable of effectively removing phenyl VOCs through the reaction-type adsorption mechanism. The effects of the solvent (water, ethyl acetate) used to impregnate silica gel with H_2SO_4 solution in order to prepare SSA adsorbents have been studied. As-prepared two series SSA(E)-x and SSA(W)-x materials (x = 1, 2, 3, 4) were characterized by TG, SEM/EDS and N_2 adsorption/desorption techniques, and their breakthrough adsorption performances were evaluated from experimental and theoretical aspects. The results showed that the H_2SO_4 loading amounts were 2.8, 4.0, 4.8 and 5.6 mmol g^{-1} respectively for both SSA(E)-x and SSA(W)-x when x equaled 1, 2, 3, 4. Among them, SSA(E)-4 was found to have a higher proportion of the C-state H_2SO_4 than SSA(W)-4. Both SSA(E)-x and SSA(W)-x exhibited significant removal capacity of gaseous *o*-xylene. The reactive temperature regions were determined to be 120–170 °C for SSA(E)-4 and 120–160 °C for SSA(W)-4 with a common optimum point of 160 °C. Both SSA(E)-x and SSA(W)-x adsorbents exhibited excellent recyclability and reuse performance. Further, the series SSA(E)-x materials outperformed the series SSA(W)-x on all adsorption performance metrics, suggesting that ethyl acetate is a preferred solvent for preparing the SSA materials in phenyl VOCs removal application.

Keywords: silica sulfuric acids; impregnation; ethyl acetate; *o*-xylene; reaction-type adsorption

1. Introduction

Volatile organic compounds (VOCs), such as acetone, dichloromethane, benzene, toluene [1], xylenes, etc., are released during production, storage, delivery and application, thus are the commonly encountered pollutants in industrial and residential environments [2]. The adverse hazards of VOCs in the environment mainly include the photochemical formation of organic aerosols, along with affecting human health by inducing respiratory system diseases, metabolic disorders, sensory irritation [3], and particularly carcinogenic risk in extreme cases [4]. Therefore, the release levels of VOCs are stringently regulated by legislation and discharge standards [5–7]. Necessarily, the purification and/or recovery issue of VOCs has attained increasing attention [8] and has been proposed as one of the most pressing research challenges of the environmental and chemical engineering fields.

Many different methods, such as condensation, liquid absorption, solid adsorption, thermal incineration, complete catalytic combustion [9] and biological degradation, have been developed to control VOCs pollution [10–14]. Among them, adsorption is a favored

technology in this field due to lower economic cost, process safety and renewable adsorbents, etc. It is known that both pressure swing adsorption (PSA) and temperature swing adsorption (TSA) are typically employed at an industrial scale, in which the regeneration of the spent adsorbent and recovery of the adsorbate can usually be performed [15–18]. However, from the principle of VOCs removal in both processes, the adsorbates are immobilized on the solid surface through physical interaction, where effective adsorption can occur only at a relatively low temperature (for TSA) or high pressure (for PSA), while the desorption needs to proceed at a high temperature or in vacuum conditions. In fact, the adsorption capacity of the adsorbents in both processes is essentially manipulated by their texture properties (specific surface area, pore volume and pore width); however, these characteristics are susceptible to deterioration because of the pore collapsing/clogging and surface contamination [19,20]. These issues often impede these increasingly popular traditional adsorption technologies. Therefore, it is immensely meaningful from both academic and applied perspectives to explore novel adsorption techniques and materials for treating VOCs.

A novel reaction-type adsorption approach was proposed by our research group to enable the resource treatment of phenyl VOCs such as benzene and xylene, which differed in principle from the traditional TSA and PSA processes, exhibiting a good promising prospect [21]. It was confirmed that the process was achieved by the sulfonation reaction of *o*-xylene on silica sulfuric acid (SSA) [21]; thus, the preparation procedure of SSA may have an important effect on the adsorptive performance. In a previous study [22], the silica supported sulfuric acid (SSAI) prepared by sol-gel processing was compared with the SSAII prepared by the impregnation method. The results showed that SSAI exhibited a higher breakthrough adsorption capacity as compared to SSAII, which contributed to a greater proportion of C-state sulfuric acid on the SSA surface. The findings above demonstrated the importance of the SSA preparation procedure. In this sense, the effect of the solvent used to impregnate silica support with H_2SO_4 on the adsorptive performance and properties of the obtained SSA materials should be further explored, and the goal of this study is to compare two solvents (water and ethyl acetate) for this purpose.

2. Results

2.1. Loading Amount and Anchoring States of Sulfuric Acid in the SSA(E)-x and SSA(W)-x

As described in Section 3.2, the preparation of the SSA(E)-x and SSA(W)-x materials consists of three operations: impregnation, rotary evaporation and drying at 100 °C. The impregnation was carried out to achieve the homogeneous distribution and infiltration of the SG support surface and pores, which were potentially affected by the features of the solvent. The rotary evaporation and drying were designed in such a way as to remove bulk and residual solvent. No difference in the loading amounts of H_2SO_4 was observed of such obtained SSA(E)-x and SSA(W)-x with same x. When x was 1, 2, 3 and 4, their loading amounts of H_2SO_4 were determined to be 2.8, 4.0, 4.8 and 5.6 mmol g^{-1} respectively. Correspondingly, the H_2SO_4 utilization ratios were calculated to be 76.1%, 54.3%, 43.5% and 38.0%, which decreased with the increasing x. This finding demonstrated that the loading amount of H_2SO_4 is co-determined by the H_2SO_4 dosage and the drying temperature but is independent of the used solvent features. However, as can be seen from Figure 1 and Table 1 (the TG curves and the calculated amount of the P- and C-state H_2SO_4 for the SSA(E)-4 and SSA(W)-4), the proportion of the C-state H_2SO_4 in SSA(E)-4 was higher than that in SSA(W)-4, indicating that the features of the solvents affected the anchoring states of sulfuric acid in SG support. As suggested in our previous studies [22,23], the C-state H_2SO_4, defined as the chemically bonded sulfuric acid, was formed by the condensation of silanol groups of SG surface and sulfuric acid molecules, and it was higher than the P-state counterpart (defined as the physisorbed sulfuric acid) in the bond strength. It was speculated that the use of ethyl acetate as the impregnation medium might promote the condensation of silanol groups and H_2SO_4 molecules since it is a weakly polar solvent (dipole moment $\mu = 4.40$, dielectric constant $\varepsilon = 6.02$) without hydroxyl groups compared

with water ($\mu = 1.84$, $\varepsilon = 80.10$) [24]. Thus, ethyl acetate led to the formation of a greater proportion of the C-state H_2SO_4, improving the adsorptive performance of SSA(E)-4 for *o*-xylene.
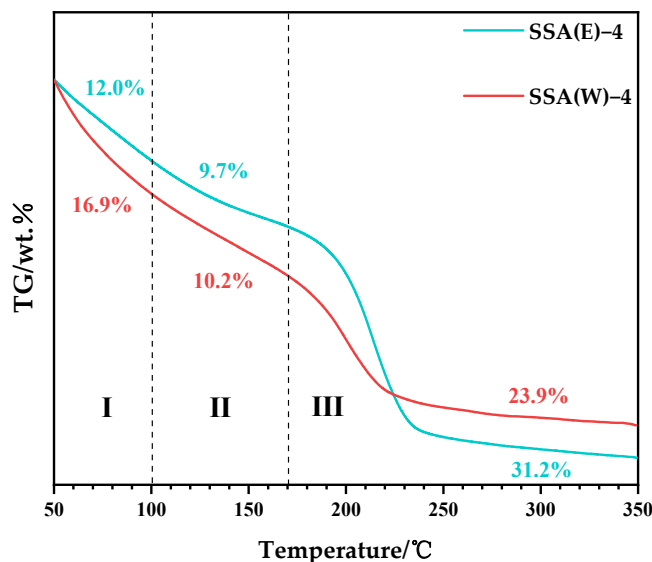

Figure 1. TG curves of SSA(E)-4 and SSA(W)-4.

Table 1. Amounts of P- and C-state sulfuric acid in SSA(E)-4 and SSA(W)-4.

T (°C)	SSA(E)-4		SSA(W)-4	
	TG (%)	Sulfuric Acid (%)	TG (%)	Sulfuric Acid (%)
100–170 (P-state)	−9.7	23.8	−10.2	29.8
170–350 (C-state)	−31.2	76.2	−23.9	70.2

2.2. Characterization of the Materials

The SEM and EDS results of the SG, SSA(E)-4 and SSA(W)-4 are shown in Figure 2. The SG support presented an irregular grain shape and uneven size, and only contained both Si and O elements (Figure 2a,a'), as these were prepared by simply grinding the commercial amorphous silica gel. The impregnation of SG with the H_2SO_4 solutions resulted in changes in morphology and composition of SSA(E)-4 and SSA(W)-4, mainly showing a rougher appearance, a particle size and an additional sulfur peak (Figure 2b,b',c,c'). The measured contents of S elemental were nearly equal in both SSA(E)-4 (3.4%) and SSA(W)-4 (3.6%) due to the same loading amount of H_2SO_4.

As shown in Figure 3, the N_2 adsorption/desorption isotherm of the SG support at −196 °C was judged as type IV proposed by IUPAC [25], indicating a mesoporous structure with 318 m^2 g^{-1} of a specific surface area, 0.92 cm^3 g^{-1} of pore volume and 5.8 nm of pore diameter. This feature provided abundant anchored sites for the H_2SO_4 molecules. When the SG support was impregnated with the H_2SO_4 solution, H_2SO_4 infiltrated into the pores and covered the surface sites (such us Si-OH). Thus, the obtained SSA(E)-4 and SSA(W)-4 were observed to have a minimal specific surface area (~7 m^2 g^{-1}) and pore volume (~0.06 cm^3 g^{-1}) (Figure 3).
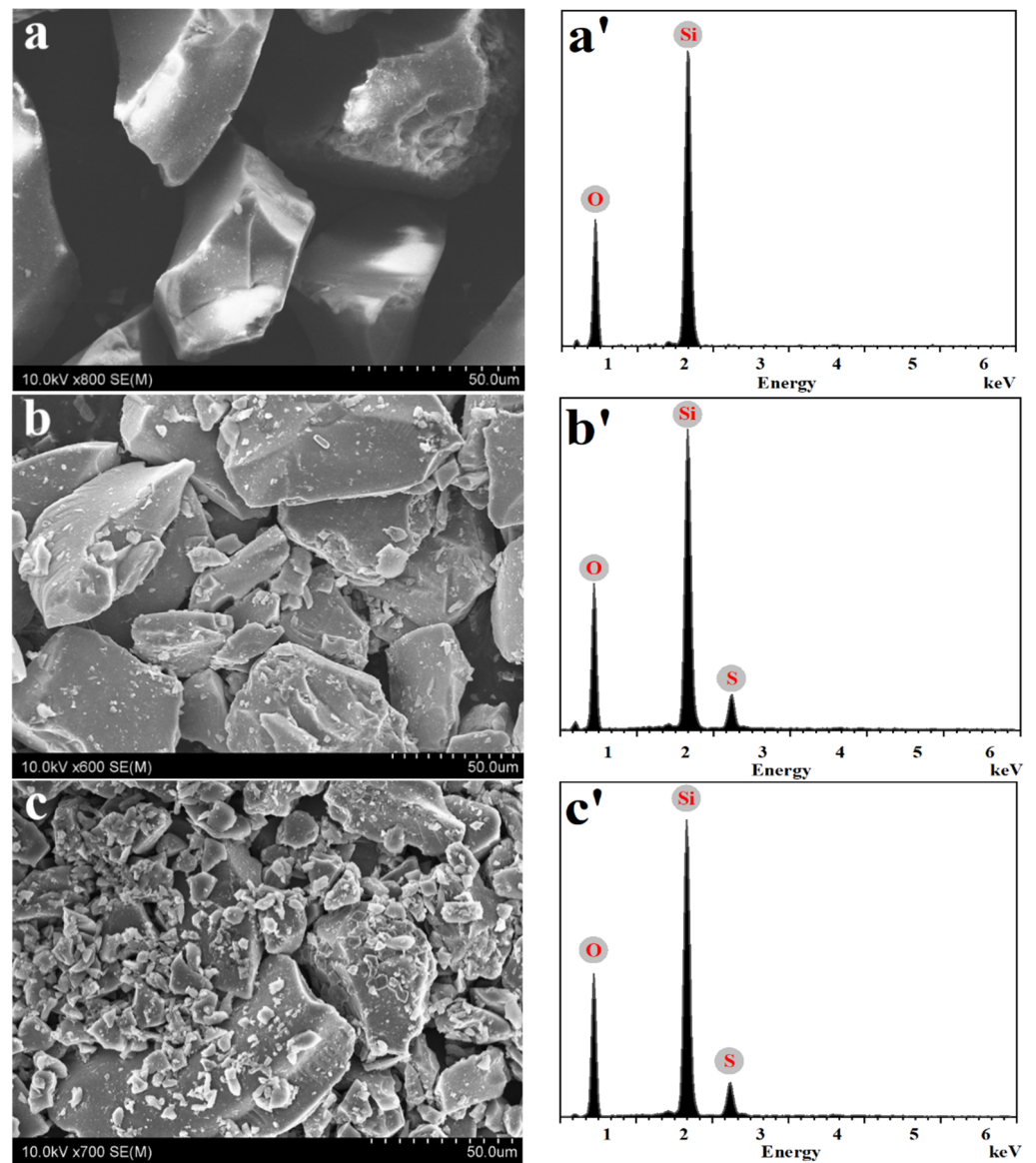
Figure 2. SEM images and EDS spectra of SG (**a**,**a'**), SSA(E)-4 (**b**,**b'**) and SSA(W)-4 (**c**,**c'**).
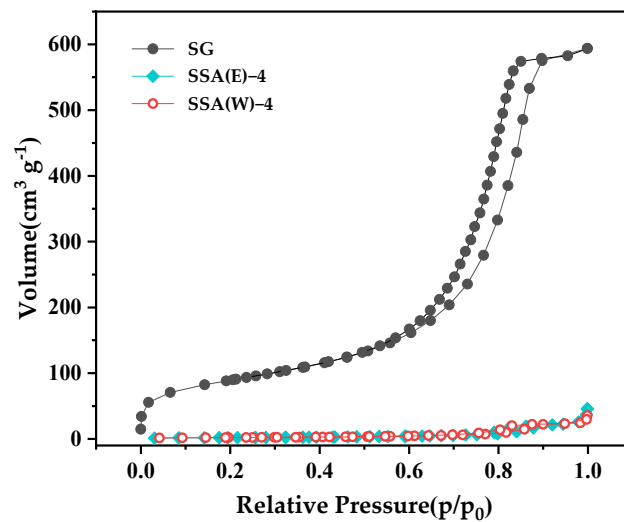

Figure 3. N_2 adsorption/desorption isotherms of SG, SSA(E)-4 and SSA(W)-4.

2.3. Effect of Temperature on Adsorption of SSA(E)-4 and SSA(W)-4 for o-Xylene

The $X_{o\text{-}x} \sim T$ curve of *o*-xylene in the SG, SSA(E)-4 and SSA(W)-4 filled beds are shown in Figure 4. As can be seen, both SSA(E)-4 and SSA(W)-4 exhibited a unique temperature region (where $X_{o\text{-}x} \geq 99\%$), while SG had no removal for *o*-xylene in the same temperature region due to the absence of anchored H_2SO_4. The methyl group on *o*-xylene has an electron-donating effect, which increases the electron density and activity of the ortho-para position of the benzene ring, and is attacked by the electrophilic group $-HSO_3$. However, due to the large space occupied by the sulfonic acid group as well as the influence of the steric hindrance effect of the methyl group, the sulfonation reaction is more likely to happen at the para position of the methyl group. This phenomenon was attributed to the reaction-type adsorption mechanism, the equations of which are shown in Scheme 1 [23]. The ending point of this reactive adsorption region of SSA(E)-4 was a little higher than that of SSA(W)-4, which was expected to be associated with a greater proportion of the C-state H_2SO_4 of SSA(E)-4. Further, the experimental dotted plots and the corresponding dose–response model [26] fitting curves for describing breakthrough adsorption behavior of *o*-xylene with both SSA(E)-4 and SSA(W)-4 at different temperatures are depicted in Figure 5. All R^2 values were close to 1 and this observation also appeared in the later results (will not be repeated), meaning good fitness of the dose–response model and satisfactory prediction efficacy. These obtained experimental metrics and fitting results are reported in Table 2. The results demonstrated that both SSA(E)-4 and SSA(W)-4 possessed superior adsorption behavior over a long duration with almost no escaping *o*-xylene molecules and the adsorption capacity varied with the bed temperature, exhibiting a maximum adsorption at 160 °C. However, at various bed temperatures, SSA(E)-4 outperformed SSA(W)-4 on all experimental (t_B, Q_B) and theoretical ($t_{B,th}$, $Q_{B,th}$) performance metrics, indicating that SSA(E)-4 was a superior adsorption material than SSA(W)-4 for the removal of *o*-xylene. It is speculated that the observed adsorption superiority of SSA(E)-4 towards *o*-xylene was closely associated with a higher amount of the C-state H_2SO_4 as compared to SSA(E)-4. Gao et al. [23] suggested that the C-state sulfuric acid had higher thermal stability than the P-state counterpart, thereby leading to a superior performance in SSA(E)-4 for removing *o*-xylene from the gas stream.
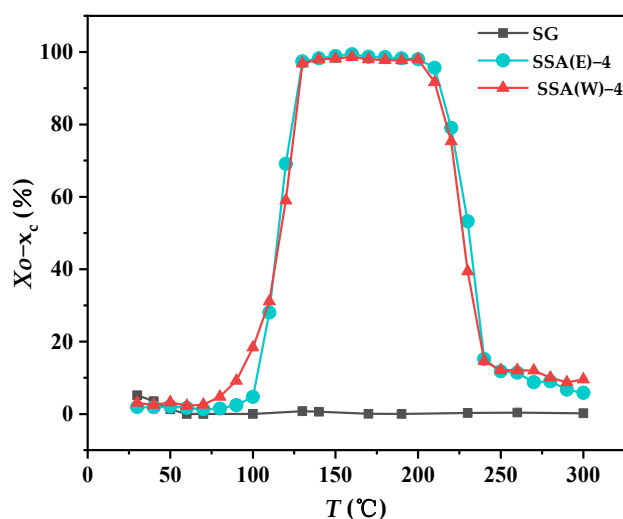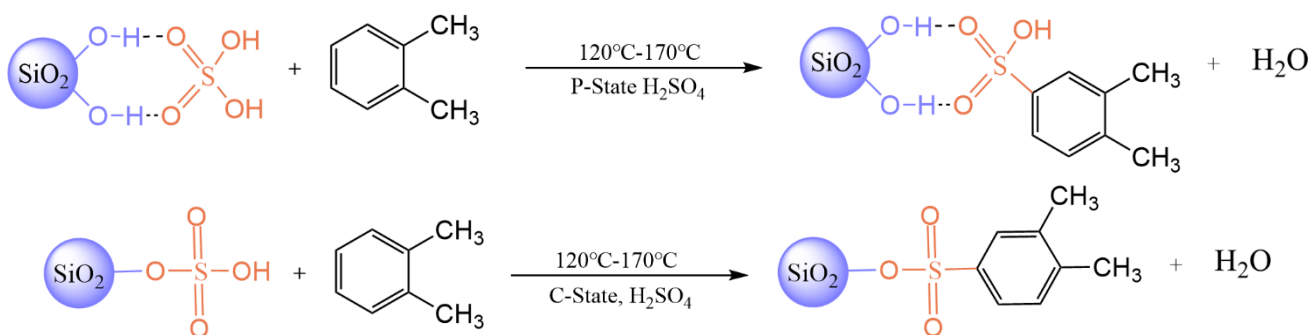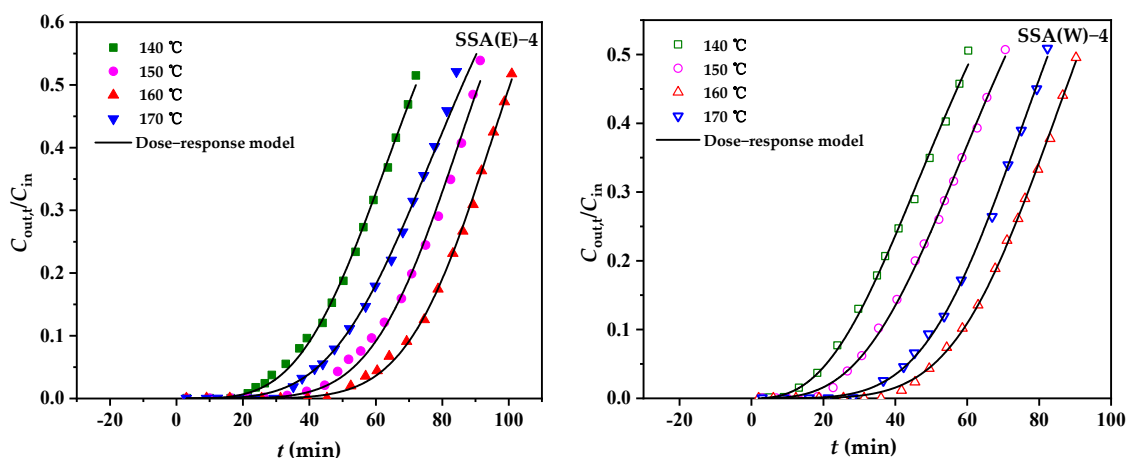

Figure 4. Plots of *o*-xylene removal ratios ($Xo\text{-}x_c$) vs. temperature (T) for SG, SSA(E)-4 and SSA(W)-4.

Scheme 1. Adsorption reaction equations of the P-state and C-state sulfuric acids with *o*-xylene.

Figure 5. Experimental dotted plots and dose-response model fitting breakthrough curves of SSA(E)-4 and SSA(W)-4.

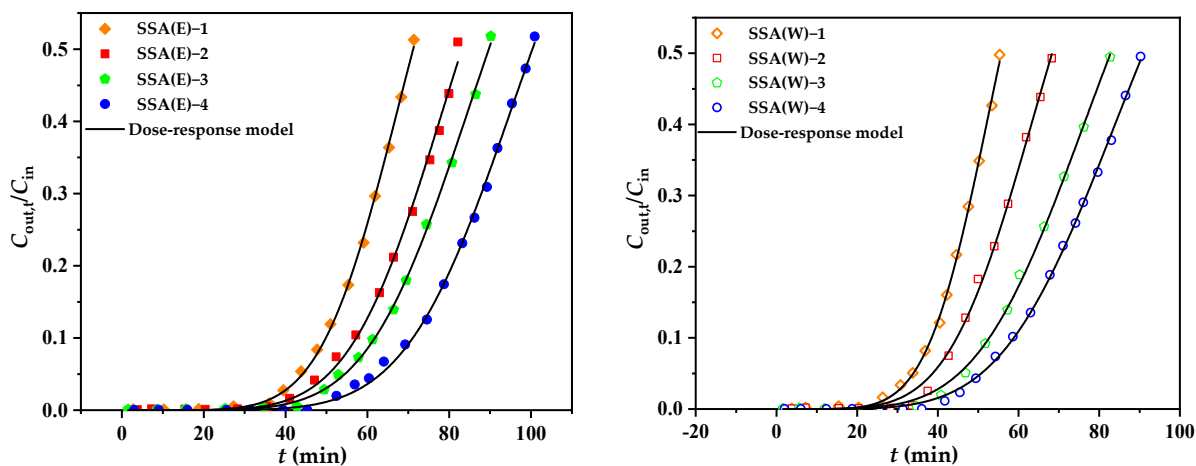**Table 2.** Experimental and fitting results at different temperatures.

	T (°C)	140	150	160	170
SSA(E)-4	t_B (min)	32.2	50.4	61.9	42.3
	Q_B (mg g^{-1})	111.2	174.4	214.7	146.4
	$t_{B,th}$ (min)	33.9	53.3	63.2	42.5
	$Q_{B,th}$ (mg g^{-1})	117.6	185.2	221.0	147.6
	q_0 (mg g^{-1})	0.2523	0.3185	0.3512	0.3012
	a	3.9182	5.1180	6.3821	4.1696
	R^2	0.9980	0.9944	0.9988	0.9919
SSA(W)-4	t_B (min)	20.4	28.4	51.9	42.9
	Q_B (mg g^{-1})	70.0	98.1	179.9	148.3
	$t_{B,th}$ (min)	20.8	28.6	50.7	43.3
	$Q_{B,th}$ (mg g^{-1})	72.5	99.3	176.5	149.4
	q_0 (mg g^{-1})	0.2154	0.2478	0.3183	0.2888
	a	2.7141	3.2536	5.0418	4.5911
	R^2	0.9979	0.9987	0.9992	0.9990

Annotation: t_B, experimental breakthrough time; $t_{B,th}$, theoretical breakthrough time; Q_B, experimental breakthrough adsorption capacity; $Q_{B,th}$, theoretical breakthrough adsorption capacity; a and q_0, dose-response model constants.

2.4. Effect of H_2SO_4 Loading Amount on Adsorption of SSA(E) and SSA(W) for o-Xylene

The breakthrough adsorption behaviors of two series of SSA(E) and SSA(W) materials with different H_2SO_4 loading amounts for *o*-xylene were investigated, as shown in Figure 6. It was observed that their breakthrough adsorption curves were shifted uniformly to the right with increasing H_2SO_4 loading amount, further demonstrating that H_2SO_4 molecules

anchored on the SG surface were responsible for *o*-xylene removal [21]. Meanwhile, at the same H$_2$SO$_4$ loading levels, SSA(E) materials were superior to SSA(W) contrasts over all adsorption performance metrics (see Table 3), suggesting that ethyl acetate was a preferred solvent for preparing the SSA materials.

Figure 6. Experimental dotted plots and dose-response model fitting breakthrough curves of SSA(E) and SSA(W) with different H$_2$SO$_4$ loading amounts.

Table 3. Experimental and fitting results at different H$_2$SO$_4$ loading amounts.

H$_2$SO$_4$ Loading Amount (mmol/g)		2.8	4.0	4.8	5.6
SSA(E)	t_B (min)	43.5	49.0	53.7	61.9
	Q_B (mg g^{-1})	151.1	169.8	186.5	214.7
	$t_{B,th}$ (min)	44.1	50.4	54.4	63.2
	$Q_{B,th}$ (mg g^{-1})	154.1	174.6	188.4	221.0
	q_0 (mg g^{-1})	0.2492	0.2908	0.3139	0.3512
	a	6.1636	5.9063	5.9061	6.3821
	R^2	0.9992	0.9972	0.9991	0.9988
SSA(W)	t_B (min)	33.4	40.3	46.9	51.9
	Q_B (mg g^{-1})	115.3	140.1	162.7	179.9
	$t_{B,th}$ (min)	33.9	38.6	45.2	50.7
	$Q_{B,th}$ (mg g^{-1})	117.7	134.7	157.9	179.0
	q_0 (mg g^{-1})	0.1952	0.2392	0.2899	0.3183
	a	5.9138	5.1736	4.8660	5.0418
	R^2	0.9990	0.9972	0.9986	0.9992

Annotation: t_B, $t_{B,th}$, Q_B, $Q_{B,th}$, a, and q_0 are same as these in Table 2.

2.5. Reusability of the Spent Supports

Figure 7 shows the adsorption/desorption/re-sulfonation cyclic results for *o*-xylene removal by both SSA(E)-4 and SSA(W)-4 materials. No significant loss was observed in Q_B of SSA(E)-4 and SSA(W)-4 over five cyclic operations, demonstrating that both SSA(E)-4 and SSA(W)-4 possessed good reusability. By comparison, SSA(E)-4 was superior to SSA(W)-4 owing to its bigger Q_B values.
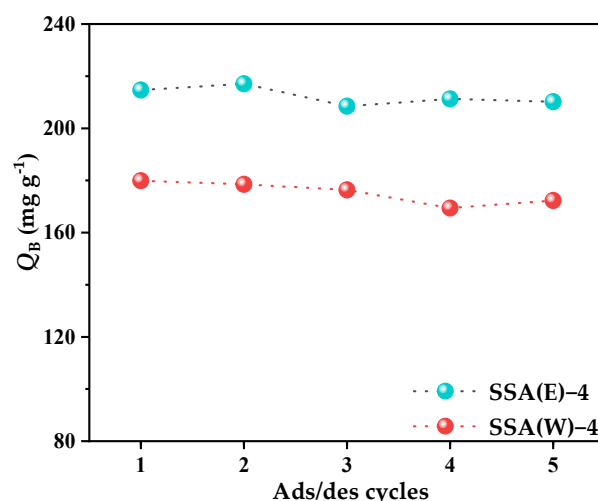
Figure 7. Reusability of SSA(E)-4 and SSA(W)-4 in the cyclic operations.

3. Materials and Methods

3.1. Materials

Silica gel (a diameter of 0.05~0.075 mm, chromatographically pure, simply referred to as SG) was purchased from the Anhui Liangchen Silicon Source Material Co. Ltd., Hefei, China. All the reagents, including ethyl acetate (99.5%), sulfuric acid (98%), *o*-xylene (99%), NaOH (96%), HCl (36–38%) and potassium hydrogen phthalate (99.8%), were analytically pure and commercially available (TianjinYongda Chemical Reagent Co. Ltd., Tianjin, China). The water was homemade deionized water (>18.2 MΩ). High purity nitrogen gas (99.999%) used as a carrying gas was procured from Shijiazhuang Xisanjiao Practical Gas Co. Ltd., Shijiazhuang, China.

3.2. Preparation Procedure of SSA

Eight SSA materials, labeled as SSA (solvent abbreviation) -x, were prepared by the H_2SO_4 solution impregnation method in water (W) or ethyl acetate (E). Here, x represented the volume (mL) of 98% H_2SO_4 added into the solvents during the impregnation. Specifically, 5 g of SG was mixed with a solution of 20 mL of the solvent and x mL of 98% H_2SO_4 in a round-bottom flask for 30 min at 30 °C. The solid precursor was separated by rotary evaporation and was then dried using an electrothermal blast oven at 100 °C for 24 h. These obtained samples were stored in a desiccator for further characterization and performance analysis. The sulfuric acid loading amount of these SSA materials was determined by NaOH standard solution titration prior to testing [23].

3.3. Characterization

The relevant characterization items of the as-prepared SSA materials were performed on S-4800 field emission scanning electron microscope (SEM) equipped with an INCA 350 energy dispersive spectrometer (EDS) (Hitachi, Chiyoda City, Japan), TENSOR 27 Fourier-transform infrared spectrometer (FTIR, KBr method; Bruker AXS, Karlsruhe, Germany), Kubo X1000 automatic surface area and pore analyzer (Beijing Builder Co., Ltd., Beijing, China), STA 449F 3TG/DSC analyzer (Netzsch, Selb, Germany) and ESCALAB 250Xi X-ray photoelectron spectrometer (XPS; Thermo Fisher, Cambridge, UK).

3.4. Dynamic Adsorption Tests

The dynamic adsorption tests of a series of the SSA(E)-x and SSA(W)-x materials were performed in a custom-made testing platform, which was described in our previous studies [27]. Before the beginning of each experiment, the testing samples (100 mg, ≤0.15 mm) were blended with an equal part of inert quartz sands (0.180–0.425 mm) and then filled in the adsorption column (6 mm i.d. × 40 cm). The *o*-xylene-containing simulated gas was

created online by the N_2 bubbling method and went through the filled bed. The gas flow rate was controlled via flow meters (Sevenstar, D07-26), and the concentration of *o*-xylene was determined on GC7900 gas chromatography apparatus with a flame ionization detector (Tianmei, Shanghai, China). To compare the adsorption behavior and performance of the SSA(E)-x and SSA(W)-x materials, the *o*-xylene removal ratios (X_{o-x}), the breakthrough time (t_B, min) and the breakthrough adsorption capacity (Q_B, mg g^{-1}) were determined at different conditions. Among the three performance metrics, t_B was defined as the time at $C_{out,t}/C_{in} = 0.05$, X_{o-x} and Q_B were calculated from Equations (1) and (2) respectively.

$$X_{O-X} = \frac{C_{in} - C_{out,t}}{C_{in}} \times 100\% \tag{1}$$

$$Q_B = \frac{VgCin}{m} \int_0^{tB} (1 - \frac{Cout,t}{Cin}) dt, \tag{2}$$

where C_{in} and $C_{out,t}$ are the inlet concentration and outlet concentration of *o*-xylene in the gas flow (mg L^{-1}) respectively, V_g is gas flow rate (mL min^{-1}), m is the amount of the adsorbent (g), t is the process time (min).

To better understand the dynamic adsorption behaviors, the dose–response model (Equation (3)) was used to fit the above experimental data and calculate both theoretical adsorption performance parameters ($t_{B,th}$/min and $Q_{B,th}$/mg g^{-1}) [27].

$$\frac{C_{out,t}}{C_{in}} = 1 - \frac{1}{1 + \left(\frac{C_{in} \times v \times t}{q0 \times m}\right)^a}, \tag{3}$$

where q_0 and a are two constants of the dose–response model.

3.5. Desorption/Regeneration Experiments

After exposure to *o*-xylene, the SSA materials were repeatedly extracted with absolute ethanol. The extracted SSA materials were washed with deionized water and dried at 100 °C. The recovered SG was subsequently re-prepared as SSA by using the earlier-described impregnation method. Here, the breakthrough adsorption experiments were performed at 160 °C with 0.10 g of sample mass under the conditions of 50 mL min^{-1} V_g and 7.0 mg L^{-1} C_{in}.

4. Conclusions

Two series SSA(E)-x and SSA(W)-x materials (x = 1, 2, 3, 4) were prepared by the H_2SO_4 solution impregnation method in water (W) and ethyl acetate (E), and their H_2SO_4 loading amounts were 2.8, 4.0, 4.8 and 5.6 mmol g^{-1} respectively. The H_2SO_4 proportions of the P-state and C-state in both SSA(E)-4 and SSA(W)-4 were determined by the TG characterization. SSA(E)-4 was noted to have a higher content of the C-state H_2SO_4 than SSA(W)-4. The dynamic adsorption results revealed that both SSA(E)-x and SSA(W)-x possessed a significant capacity for the removal of the gaseous *o*-xylene, attributed to the reaction-type adsorption between *o*-xylene and anchored sulfuric acid. The optimum temperatures for both SSA(E)-4 and SSA(W)-4 were determined to be 160 °C. Both SSA(E)-x and SSA(W)-x adsorbents exhibited excellent recyclability and reuse performance over five consecutive adsorption/regeneration cycles. Further, the series SSA(E)-x materials outperformed the series SSA(W)-4 on all adsorption performance metrics. The results suggested that ethyl acetate was a preferred solvent for preparing the SSA materials in phenyl VOCs removal application.

References

1. Sonar, S.; Giraudon, J.M.; Veerapandian, S.K.P.; Lamonier, J.F.; Morent, R.; Lofberg, A.; De Geyter, N. Adsorption followed by plasma assisted catalytic conversion of toluene into CO_2 on hopcalite in an air stream. *Catalysts* **2021**, *11*, 845. [CrossRef]

2. Sui, H.; Liu, H.; An, P.; He, L.; Li, X.; Cong, S. Application of silica gel in removing high concentrations toluene vapor by adsorption and desorption process. *J. Taiwan Inst. Chem. Eng.* **2017**, *74*, 218–224. [CrossRef]

3. Bernstein, J.A.; Alexis, N.; Bacchus, H.; Bernstein, I.L.; Fritz, P.; Horner, E.; Li, N.; Mason, S.; Nel, A.; Oullette, J.; et al. The health effects of non-industrial indoor air pollution. *J. Allergy Clin. Immunol.* **2008**, *121*, 585–591. [CrossRef] [PubMed]

4. Saldarriaga, J.F.; Aguado, R.; Morales, G.E. Assessment of VOC emissions from municipal solid waste composting. *Environ. Eng. Sci.* **2014**, *31*, 300–307. [CrossRef]

5. Feron, V.J.; Til, H.P.; De Vrijer, F.; Van Bladeren, P.J. Review: Toxicology of volatile organic compounds in indoor air and strategy for further research. *Indoor. Built Environ.* **1992**, *1*, 69–81. [CrossRef]

6. Huang, H.; Xu, Y.; Feng, Q.; Leung, D.Y.C. Low temperature catalytic oxidation of volatile organic compounds: A review. *Catal. Sci. Technol.* **2015**, *5*, 2649–2669. [CrossRef]

7. Rochard, G.; Olivet, L.; Tannous, M.; Poupin, C.; Siffert, S.; Cousin, R. Recent advances in the catalytic treatment of volatile organic compounds: A review based on the mixture effect. *Catalysts* **2021**, *11*, 1218. [CrossRef]

8. Veerapandian, S.K.P.; De Geyter, N.; Giraudon, J.M.; Lamonier, J.F.; Morent, R. The use of zeolites for VOCs abatement by combining non-thermal plasma, adsorption, and/or catalysis: A review. *Catalysts* **2019**, *9*, 98. [CrossRef]

9. Kim, H.S.; Kim, H.J.; Kim, J.H.; Kim, J.H.; Kang, S.H.; Ryu, J.H.; Park, N.K.; Yun, D.S.; Bae, J.W. Noble-metal-based catalytic oxidation technology trends for volatile organic compound (VOC) removal. *Catalysts* **2022**, *12*, 63. [CrossRef]

10. Zhang, X.; Gao, B.; Creamer, A.E.; Cao, C.; Li, Y. Adsorption of VOCs onto engineered carbon materials: A review. *J. Hazard. Mater.* **2017**, *338*, 102–123. [CrossRef]

11. Wu, Y.; Lu, Y.; Song, C.; Ma, Z.; Xing, S.; Gao, Y. A novel redox-precipitation method for the preparation of α-MnO_2 with a high surface Mn^{4+} concentration and its activity toward complete catalytic oxidation of *o*-xylene. *Catal. Today* **2013**, *201*, 32–39. [CrossRef]

12. Ma, Z.; Zhu, L.; Lu, X.; Xing, S.; Wu, Y.; Gao, Y. Catalytic ozonation of p-nitrophenol over mesoporous Mn–Co–Fe oxide. *Sep. Purif. Technol.* **2014**, *133*, 357–364. [CrossRef]

13. Wu, Y.; Feng, R.; Song, C.; Xing, S.; Gao, Y.; Ma, Z. Effect of reducing agent on the structure and activity of manganese oxide octahedral molecular sieve (OMS-2) in catalytic combustion of *o*-xylene. *Catal. Today* **2017**, *281*, 500–506. [CrossRef]

14. Zhu, L.; Shen, D.; Luo, K.H. A critical review on VOCs adsorption by different porous materials: Species, mechanisms and modification methods. *J. Hazard. Mater.* **2020**, *389*, 122102. [CrossRef]

15. Dammak, N.; Fakhfakh, N.; Fourmentin, S.; Benzina, M. Treatment of gas containing hydrophobic VOCs by adsorption process on raw and intercalated clays. *Res. Chem. Intermed.* **2014**, *41*, 5475–5493. [CrossRef]

16. Ambrożek, B.; Zwarycz-Makles, K. Theoretical and experimental studies of the recovery of volatile organic compounds from waste air streams in the thermal swing adsorption system with closed-loop regeneration of adsorbent. *Energ. Convers. Manag.* **2014**, *85*, 646–654. [CrossRef]

17. Ramalingam, S.G.; Pre, P.; Giraudet, S.; Le Coq, L.; Le Cloirec, P.; Baudouin, O.; Dechelotte, S. Different families of volatile organic compounds pollution control by microporous carbons in temperature swing adsorption processes. *J. Hazard. Mater.* **2012**, *221*, 242–247. [CrossRef]

18. Swetha, G.; Gopi, T.; Chandra, S.S.; Ramakrishna, C.; Saini, B.; Rao, P.V.L. Combination of adsorption followed by ozone oxidation with pressure swing adsorption technology for the removal of VOCs from contaminated air streams. *Chem. Eng. Res. Des.* **2017**, *117*, 725–732. [CrossRef]

19. Meng, Z.; Liu, Y.; Li, X.; Ma, Z. Removal of siloxane (L2) from biogas using methyl-functionalised silica gel as adsorbent. *Chem. Eng. J.* **2020**, *389*, 124440. [CrossRef]

20. Pak, S.H.; Jeon, M.J.; Jeon, Y.W. Study of sulfuric acid treatment of activated carbon used to enhance mixed VOC removal. *Int. Biodeter. Biodegr.* **2016**, *113*, 195–200. [CrossRef]

21. Dong, Y.; Liu, Y.; Wang, J.; Gao, K.; Ma, Z. Silica supported sulfuric acid for the removal of gaseous *o*-xylene. *J. Environ. Chem. Eng.* **2019**, *7*, 102992. [CrossRef]

22. Ma, M.; Gao, K.; Ma, Z.; Ding, J. Influence of preparation method on the adsorptive performance of silica sulfuric acid for the removal of gaseous *o*-xylene. *Sep. Purif. Technol.* **2021**, *265*, 118484. [CrossRef]

23. Gao, K.; Ma, M.; Liu, Y.; Ma, Z. A comparative study of the removal of *o*-xylene from gas streams using mesoporous silicas and their silica supported sulfuric acids. *J. Hazard. Mater.* **2021**, *409*, 124965. [CrossRef] [PubMed]

24. Mollasalehi, H.; Yazdanparast, R. Non-crosslinking gold nanoprobes for detection of nucleic acid sequence-based amplification products. *Anal. Biochem.* **2012**, *425*, 91–95. [CrossRef] [PubMed]

25. Bi, L.; Chen, Z.; Li, L.; Kang, J.; Zhao, S.; Wang, B.; Yan, P.; Li, Y.; Zhang, X.; Shen, J. Selective adsorption and enhanced photodegradation of diclofenac in water by molecularly imprinted TiO_2. *J. Hazard. Mater.* **2021**, *407*, 124759. [CrossRef] [PubMed]

26. Fakhfakh, N.; Dammak, N.; Benzina, M. Breakthrough modeling and experimental design for *o*-xylene dynamic adsorption onto clay material. *Environ. Sci. Pollut. Res.* **2018**, *25*, 18263–18277. [CrossRef] [PubMed]

27. Ma, M.; Gao, K.; Zhao, D.; Ma, X.; Ma, Z. Effect of process conditions on reaction-type adsorption of *o*-xylene by MCM-41 supported sulfuric acid: Model simulations of breakthrough curves. *J. Environ. Chem. Eng.* **2022**, *10*, 106937. [CrossRef]